Smooth Nanowire/Polymer Composite Transparent Electrodes

*Whitney Gaynor, George F. Burkhard, Michael D. McGehee, and Peter Peumans**

Transparent electrodes are critical components of thin-film optoelectronic devices such as displays and thin-film solar cells. Most high-performance transparent conducting films in use today are composed of sputtered metal oxides.[1,2] These films can have sheet resistances under 20 $\Omega\ \square^{-1}$ with 90% transmission when deposited at a high temperature onto glass and resistances increasing to 40–200 $\Omega\ \square^{-1}$ with the same transmission when deposited at lower temperatures onto plastic substrates.[2,3] Recent research has focused on replacing conductive metal oxides with alternative materials that can be deposited from solution and can reproduce the performance of metal oxides on glass on various substrates, including plastics. In addition, metal oxides are brittle,[4,5] and thus alternative transparent conductor technologies are also focusing on flexibility and robustness to enable lightweight, flexible solar cells and other thin film devices.

Strategies for non-vacuum deposition of transparent electrodes make use of materials other than metal oxides[6] including carbon nanotubes,[7–12] reduced graphene oxide,[13–16] films using both carbon components,[17] highly conductive poly-(4,3-ethylene dioxythiophene):poly(styrene-sulfonate) (PEDOT:PSS),[18–23] electrospun copper networks,[24] printed metal grids,[25–27] and Ag nanowire films.[28–32] Most of these alternatives do not currently match the performance of conductive oxides. In particular, the solution-processed carbon-based materials listed above have sheet resistances much higher than those of metal oxides at comparable optical transmission, from 100 to 5000 $\Omega\ \square^{-1}$.[6–23] This corresponds to figures of merit, defined by the ratio of the DC conductivity to the absorption coefficient, σ/α,[33] of 0.07 Ω^{-1} to $1.3 \times 10^{-3}\ \Omega^{-1}$. To avoid significant losses in solar cell efficiency brought about by the transparent electrode, the values for these figures of merit should be as high as possible, ideally above 1 Ω^{-1}.[33] At this point in development, Ag nanowire films already demonstrate sheet resistances and transparencies comparable to metal oxides. However, they have been found to be unsuitable for many device applications due to their inherent roughness. For example, high-efficiency thin-film bulk heterojunction organic photovoltaic (OPV) cells have never been reported using Ag nanowire electrodes,[28,29,32] and bilayer evaporated devices show performance below the efficiencies for these devices fabricated on indium tin oxide (ITO).[28,32,34] In every case, low shunt resistances were observed, which corresponded to low fill factors and low efficiencies. In each case, spin-cast layers of conductive polymer coating these wires was not enough to overcome the large peaks and valleys created by the wire–wire junctions. Thus, surface roughness is clearly another factor, in addition to transparency and conductivity, that affects the device compatibility of transparent electrodes. As in some other publications, we use OPV cells to evaluate the performance of the transparent electrodes. In recent years, the efficiency of OPV has increased dramatically. The widely studied regioregular poly-(3-hexylthiophene) and C61 butyric acid methyl ester (P3HT:PCBM) bulk heterojunction has produced solar cell efficiencies over 4%.[35–37] Newer polymers with broader absorption have produced cells with efficiencies over 6%.[38,39]

In this work, we prove that the Ag nanowire mesh roughness is the reason these films are incompatible with efficient devices, and we solve this significant morphology issue, transforming the promise of Ag nanowire films into truly effective transparent electrodes. We achieve this by creating an organic–inorganic composite, embedding Ag nanowires into the conducting polymer PEDOT:PSS. By varying the polymer thickness, we are able to gain precise control of the nanoscale morphology of the composites via lamination. The aim was to embed the thick junctions between wires away from the top surface of the electrode such that the active layers in any device fabricated on top would not undergo local thinning, which would lead to shunting or shorting, while keeping the conductive mesh on the composite surface. This not only fills the gaps between the nanowires, but also creates a uniform surface profile in which the nanowires only ever rise above the polymer by one-fourth of their diameter. The technique results in smooth, solution-processed transparent conducting films that have sheet resistances and transmissivities comparable to ITO on glass and better than ITO on plastic. However, the most important feature of these electrodes is the low roughness that leads to thin-film device compatibility. We are able to produce high-efficiency P3HT:PCBM solar cells with PEDOT:PSS/Ag nanowire anodes that have the same performance metrics as those fabricated on ITO on glass. By fabricating the composites and devices on flexible substrates, we also show that PEDOT:PSS/Ag nanowire films have superior mechanical and electrical properties to ITO on plastic, and we are able to demonstrate an increase in flexible OPV cell efficiency using these composites.

Dr. W. Gaynor, Prof. M. D. McGehee
Department of Materials Science and Engineering
Stanford University
Stanford, CA 94305, USA
Prof. P. Peumans
Department of Electrical Engineering
Stanford University
Stanford, CA 94305, USA
E-mail: ppeumans@stanford.edu
G. F. Burkhard
Department of Applied Physics
Stanford University
Stanford, CA 94305, USA

DOI: 10.1002/adma.201100566

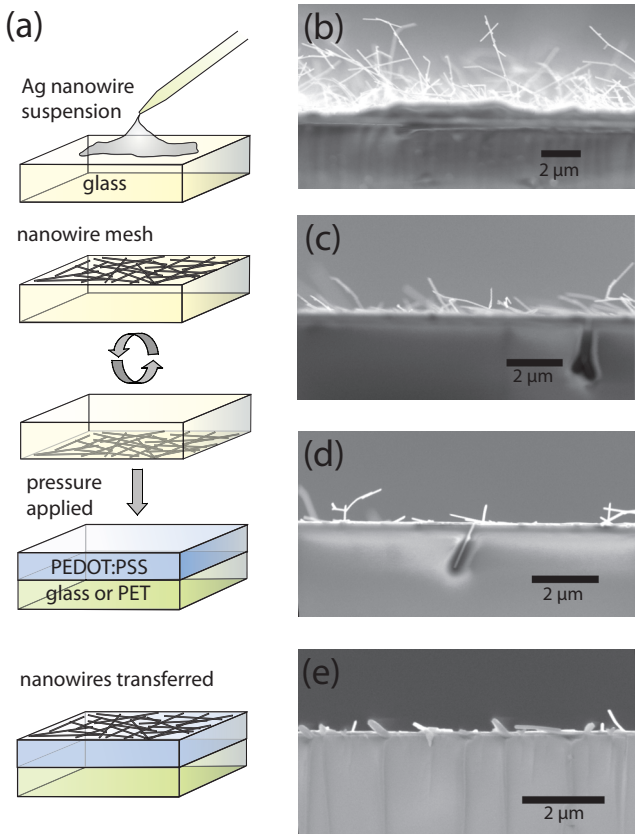

Figure 1. a) Transparent electrode fabrication procedure. b–e) Cross-section SEM images of silver nanowires laminated under the same conditions onto varying thicknesses of PEDOT:PSS: b) 25 nm, c) 50 nm, d) 75 nm, and e) 100 nm.

Films of 50- to 100-nm-diameter Ag nanowires were drop-cast from suspension onto glass.[28,30] The nanowires were then laminated onto spin-cast PEDOT:PSS films of varying thickness in order to investigate the morphology of the composites. The fabrication process is illustrated in **Figure 1**a. In all cases the same pressure was used and the wires transferred completely to the polymer. Figure 1b–e show cross-sectional scanning electron microscopy (SEM) images of nanowires embedded into four different thicknesses of PEDOT:PSS: 25 nm (b), 50 nm (c), 75 nm (d), and 100 nm (e). There are no observable differences in the resulting films to the eye, nor are there apparent differences in top view SEM images. However, cross-sectional SEM images reveal that as the PEDOT:PSS thickness increases, the composite morphology changes dramatically. On 25 nm of PEDOT:PSS, the nanowires transfer to the PEDOT:PSS but do not sink into the polymer along their lengths, resulting in a forest-like structure. As the PEDOT:PSS layer increases to 50, 75, and 100 nm, the wires sink into the PEDOT:PSS and the meshes become flatter, with the polymer filling the deep spaces between the wires. In order to create completely flat films for use as electrodes, the PEDOT:PSS needs to be thick enough to embed both single wires and the wire–wire junctions that are essential to conductivity.

Figure 2 shows SEM images of Ag nanowires laminated into 125 nm of PEDOT:PSS, which results in a transparent,

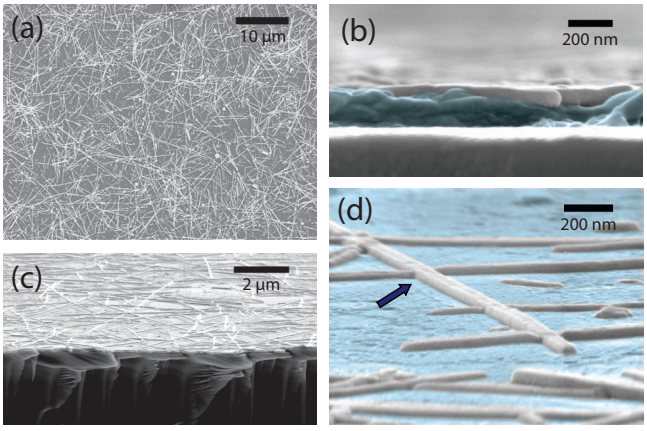

Figure 2. SEM images of composite electrodes using 125 nm of PEDOT:PSS. a) Top view. b) Cross-section. c) Angled cross-section. d) Close-up angled surface showing junctions of nanowires embedded into the polymer (indicated by arrow).

conductive, composite film with a surface flat enough for use as an electrode. A top view SEM image is shown (Figure 2a). Using image-processing software, we determined that the Ag nanowires cover 29% of the film. Cross-sectional SEM images (Figure 2b, colorized for clarity) show that the nanowires are nearly completely embedded into the PEDOT:PSS. An off-angle cross-section (Figure 2c) shows that all wires are in the plane of the substrate and appear fully connected. Figure 2d (colorized for clarity) confirms that the wire–wire junctions, indicated with an arrow, are embedded into the PEDOT:PSS layer, allowing the upper wires to stay flush. This is particularly critical for high-efficiency OPV performance, as any conductive nanostructures protruding toward the bulk heterojunction active layer will form preferential current pathways through the device, leading to shunting and a reduced fill factor.[28,30] Thus it is imperative that the wire–wire junctions, the thickest parts of the nanowire mesh, are embedded with the roughness protruding away from the device to prevent this from occurring.

Tapping mode atomic force microscopy (AFM) was used to further characterize the composite's surface morphology. The AFM topographical image of the PEDOT:PSS/Ag nanowire film is shown in **Figure 3**. The root mean square (RMS) roughness was measured at 11.9 nm, with the nanowires rising between 20 and 30 nm above the PEDOT:PSS surface, as shown in the line scan in Figure 3. This is in contrast to bare Ag nanowires, in which top-to-bottom height can be as large as 200–300 nm, depending on the number of wires stacked in junctions. The wire used in the line scan is denoted by the dark blue box in the topographical image. We note that while the maximum and minimum heights are accurate, the bell-shape of the line scan does not reflect the actual topography (see Figure 2d), but is an artifact of the AFM scan. For comparison, the RMS roughness of ITO films was measured at <3 nm, substantially smaller than the value for these composites. However, as will be shown using OPV device data, this amount of roughness in the composites does not impair the preparation of high-quality devices.

Sheet resistance and optical transmission measurements were taken to compare the performance of the composite films

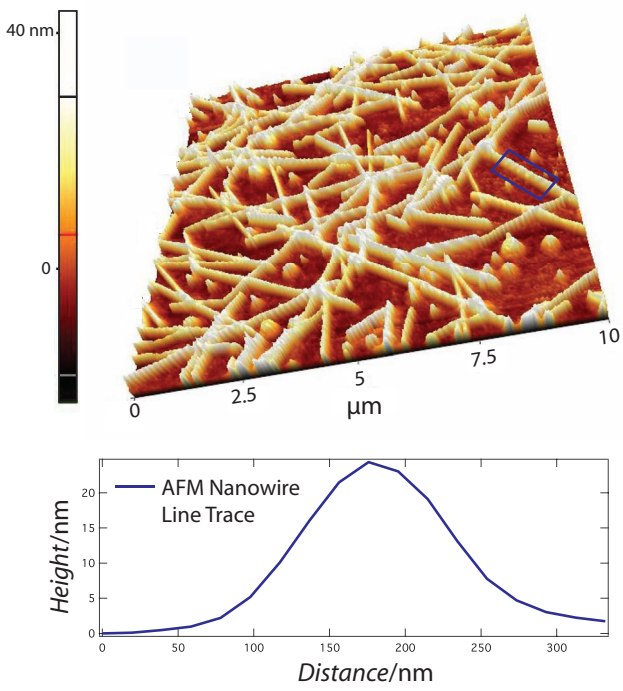

Figure 3. Tapping mode AFM scan of the PEDOT:PSS/Ag nanowire surface (top) and AFM height line profile of a nanowire (bottom). The wire used in the line scan is indicated by the dark blue box in the topographical image.

to that of ITO. Samples were prepared on glass and on 5-mil polyethylene terephthalate (PET). On glass, the ITO sheet resistance was 20 Ω □$^{-1}$, while the PEDOT:PSS/Ag nanowire composite from Figure 2 was 12 Ω □$^{-1}$. On PET, there was a larger difference between the films; the ITO sheet resistance was 42 Ω □$^{-1}$ whereas the PEDOT:PSS/Ag nanowire film was only 17 Ω □$^{-1}$. Because no high-temperature processing steps are required in the composite film fabrication, the sheet resistance is nearly substrate-independent. Sheet resistance measurements of 125 nm of PEDOT:PSS result in values greater than 10 MΩ □$^{-1}$. This means that the PEDOT:PSS is not conducting over large scales, and the bulk of the composite conductivity occurs in the nanowires.

Transmission measurements were taken with the light incident through the substrate. An integrating sphere was used to collect direct and diffuse transmission, as it has been shown that 17–20% of the light transmitted through Ag nanowires is diffuse.[28,30] The transmission values reported here do not include substrate reflections. The average transmission of ITO on glass (20 Ω □$^{-1}$) over wavelengths 350–800 nm is 90% (**Figure 4**a). The PEDOT:PSS/Ag nanowire composite (12 Ω □$^{-1}$) on glass has an average transmission of 86%. Comparing the two figures of merit, $\sigma/\alpha_{GLASS/ITO}$ = 0.50 Ω^{-1} and $\sigma/\alpha_{GLASS/PEDOT/NW}$ = 0.60 Ω^{-1}, and thus the composite is the better performing film overall. On PET, the transmission spectrum of the ITO is very different, as the ITO transmission varies with thickness and the manufacturing process. The average transmission of this ITO on plastic is 91%, although the standard deviation is much greater than on glass. The PEDOT:PSS/Ag nanowire film on plastic shows a lower average transmission at 83%, although it is important to note that the spectral response of the composites is far more substrate-independent than that of ITO. This time, comparing the figures of merit, $\sigma/\alpha_{PET/ITO}$ = 0.26 Ω^{-1} and $\sigma/\alpha_{PET/PEDOT/NW}$ = 0.34 Ω^{-1}, and again the composite performs better than ITO. The 3% lower transmission for this sample as compared to the one on glass can be attributed to variations in the nanowire suspension. The slightly lower transmission in the PEDOT:PSS/Ag nanowire composite as compared to ITO is in large part due to parasitic absorption in the PEDOT:PSS layer. The transmission spectrum of a 125-nm PEDOT:PSS layer alone has an average value of 95.5% over the spectral range.

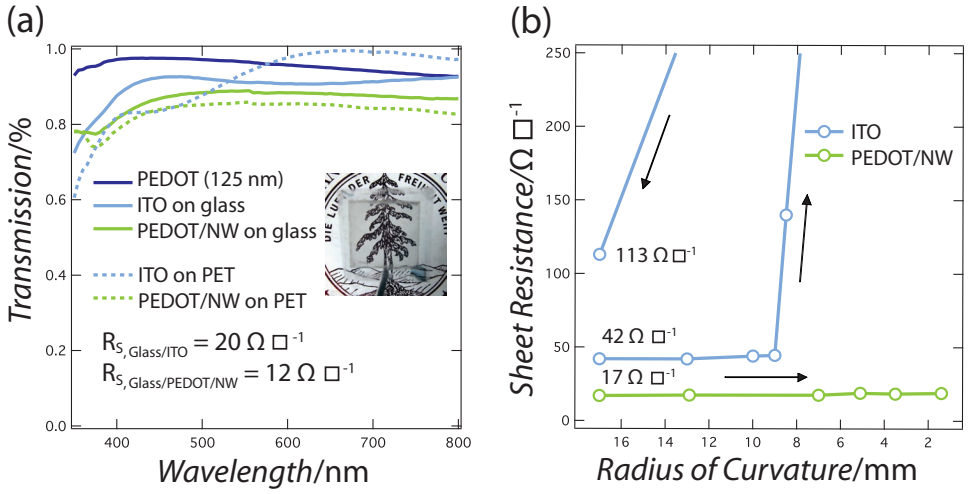

Figure 4. a) Transmission over the wavelengths 350–800 nm for ITO on glass (light blue solid) and on plastic (light blue dashed), 125-nm PEDOT:PSS on glass (dark blue), and 125-nm PEDOT:PSS with nanowires on glass (green solid) and on plastic (green dashed). ITO and PEDOT:PSS/Ag nanowires sheet resistances on glass are noted. Inset of (a) shows the PEDOT:PSS/Ag nanowire film (inner square) on plastic in front of the Stanford University seal. b) Sheet resistance vs radius of curvature for ITO (blue) and PEDOT:PSS/Ag nanowires (green) on PET. Sheet resistance values for flat films are noted.

This accounts for the lower transmissivity obtained here compared to previous studies of Ag nanowires.[28–30] The photograph in Figure 4a demonstrates the transmission of PEDOT:PSS/Ag nanowires on plastic with the Stanford University seal visible behind the inner square where the film is located.

The composites are also far more resilient to mechanical stress than ITO. To demonstrate this, films fabricated on flexible substrates were bent while the sheet resistance was measured. In Figure 4b, the sheet resistance of an ITO film on 5-mil PET (Sigma-Aldrich) is compared to that of a PEDOT:PSS/Ag nanowire composite prepared on 5-mil PET (Southwall Technologies) as a function of the substrate bending radius. The ITO sheet resistance increases significantly and irreversibly when a bending radius of 8.5 mm is reached. At an 8.5 mm bending radius and 0.75% strain, the sheet resistance increased to over 100 Ω $\square^{-1}$ and then to over 500 Ω $\square^{-1}$, before the film was re-flattened and the resistance dropped to its final value of 113 Ω $\square^{-1}$. This hysteretic behavior is consistent with ITO cracking under tension that has been previously observed.[4,5] In contrast, the same experiment does not significantly alter the sheet resistance of the composite electrodes, even at a bending radius of 1.2 mm. At a 1.2 mm bending radius and 3.5% strain, the sheet resistance of the composite went from 17 Ω $\square^{-1}$ to 18 Ω $\square^{-1}$, and the slight change can be attributed to scratches in the film induced by the measurement setup.

Bulk heterojunction photovoltaic cells using P3HT:PCBM were fabricated on ITO and on PEDOT:PSS/Ag nanowire films on both glass and plastic substrates. For comparison, the same devices were also built on bare Ag nanowire films on glass. All transparent conductors served as device anodes. Current density vs voltage for devices on glass/ITO, on glass/bare Ag nanowires, and on glass/PEDOT:PSS/Ag nanowires in the dark and under 100 mW cm^{-2} AM 1.5G illumination are shown in **Figure 5**a. On glass/ITO, the open circuit voltage was 0.625 V, the short circuit current density was 10.4 mA cm^{-2}, the fill factor was 0.65, and the power conversion efficiency was 4.2%. On glass/Ag nanowires, the cell performance decreased substantially. The open circuit voltage was 0.415 V, the short circuit current density was 2.8 mA cm^{-2}, and the fill factor was 0.25, resulting in a 0.3% power conversion efficiency. This curve is representative of the performance of all P3HT:PCBM devices made on bare nanowires in this study, with significant shunting and a poor fill factor. The optimal active layer morphology and phase separation in bulk heterojunction OPV is critical to all points of operation.[36,40,41] The cell performance and controlled fabrication indicate that the morphology required for high efficiency cannot be achieved on rough Ag nanowires. This clearly demonstrates why bare Ag nanowire films are not a suitable ITO replacement despite having low sheet resistance and high optical transmission. This is not the case for the composite films. On glass/PEDOT:PSS/Ag nanowires, the open circuit voltage was 0.615 V, the short circuit current density was 10.4 mA cm^{-2}, and the fill factor was 0.65, yielding the same power conversion efficiency, 4.2%, as the device on ITO. There is no significant difference in device performance in any metric from the ITO device and these efficiencies, at above 4%, are on par with the best cells reported using these materials.[35–37] The high fill factor is particularly noteworthy for the devices fabricated on the composites. As is evident from the current density vs voltage characteristics in Figure 5a, no shunting is present. This is a direct result of the reduced roughness brought about by embedding the wire–wire junctions away from the active layer via lamination. These devices are the highest-efficiency ITO-free OPV cells yet reported.

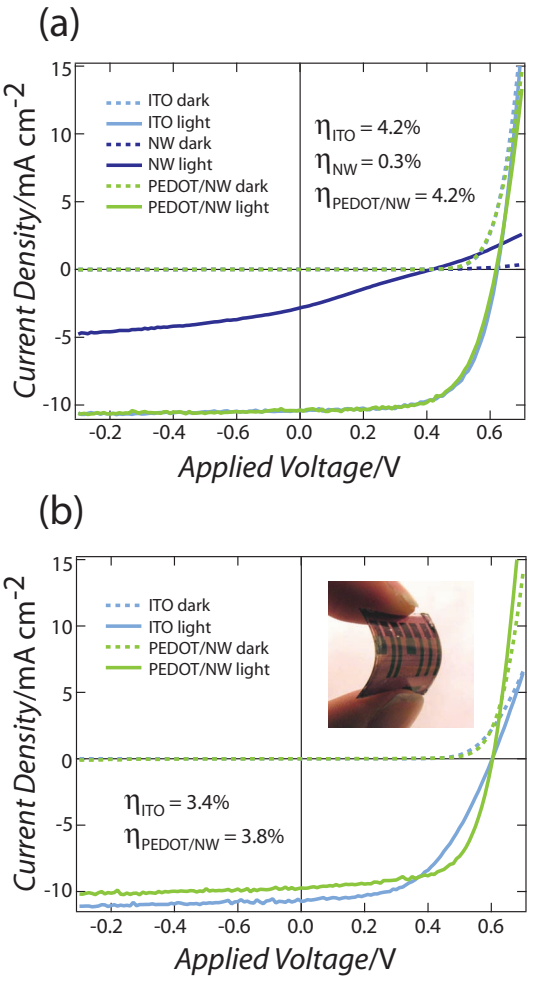

Figure 5. Current density vs voltage for P3HT:PCBM solar cells on ITO (light blue), on Ag nanowires (dark blue), and on PEDOT:PSS/Ag nanowires (green) in the dark (dashed) and under 100 mW cm^{-2} of AM 1.5G illumination (solid) on glass (a) and on plastic (b). Inset of (b) shows the P3HT:PCBM solar cell fabricated on plastic/PEDOT:PSS/Ag nanowires viewed through the substrate.

Figure 5b shows current density vs voltage for devices on plastic substrates on ITO and PEDOT:PSS/Ag nanowires in the dark and under 100 mW cm^{-2} AM 1.5G illumination. The inset shows flexible devices on PEDOT:PSS/Ag nanowires viewed through the substrate. In this case, the open circuit voltage for both devices is 0.605 V. Due to greater ITO transparency, that device has a higher short circuit current density, 10.8 mA cm^{-2}, compared to 9.74 mA cm^{-2} for the PEDOT:PSS/Ag nanowire device. However, because the composite sheet resistance is lower, the fill factor is raised from 0.52 on ITO to 0.64. This increases the efficiency from 3.4% on ITO on plastic to 3.8% on PEDOT:PSS/Ag nanowires on plastic. This is an advance toward the promise of high-efficiency flexible roll-to-roll fabricated OPV

cells. Based on these results, we anticipate the use of these composites in other types of rigid and flexible organic solar cells.

In conclusion, we have produced and characterized a truly effective ITO replacement for OPV cells by embedding Ag nanowires into conducting polymer. This raises the OPV performance with respect to rough Ag nanowire electrodes to produce high-quality devices on par with or better than those fabricated using ITO. The composites have nearly substrate-independent properties and they require no vacuum or high-temperature processing, while being able to tolerate >5 times larger mechanical strain than ITO due to substrate bending. In addition, the concept and technique presented here could be used with other nanoscale materials and polymers to create a new class of embedded nanostructure/polymer hybrid materials with novel properties. This technology, combined with the recent advances in solar cell efficiency,[38,39] could help flexible OPVs to become commercially competitive.

Experimental Section

Electrode Fabrication: All glass (VWR) and plastic (Southwall Technologies) substrates were cleaned using detergent, deionized water, acetone, and boiling isopropyl alcohol, then treated with UV-ozone for 25 min. Clevios AI 4083 (H. C. Starck) in aqueous suspension was used in all electrodes fabricated in this work. It was spun onto substrates in air at 5000, 3000, 1500, 1000, and 700 rpm to produce PEDOT:PSS films of varying thickness. These films were then annealed at 150 °C for 20 min to evaporate any remaining water. Ag nanowire films were drop-cast from suspension in methanol onto clean glass treated with poly-L-lysine (Ted Pella). These films were allowed to slowly dry on a shaking plate to prevent wire aggregation and then annealed at 180 °C for 1 h to reduce sheet resistance. All lamination was carried out in air at room temperature using a shop press (Torin) at 2.4×10^4 psi.

Electrode Characterization: Sheet resistance measurements were taken by evaporating silver pads onto the electrode surface to define a patterned square area, over which the resistance was measured using a multimeter. Transmission was measured using a monochromator, integrating sphere, and silicon photodiode (Newport). A Sirion SEM was used for imaging and Adobe Photoshop was used for the coloring of Figure 2. A Park XE-70 AFM was used in tapping mode for topography characterization.

Device Fabrication: Pre-patterned ITO substrates were used, while composite electrodes were patterned using acetone prior to device deposition. ITO was cleaned using the method described above, including UV-ozone treatment. In all cases, a 50-nm-thick PEDOT:PSS film (Clevios AI 4083, H. C. Starck) was deposited by spin-coating at 2000 rpm, followed by a 200-nm-thick photoactive layer cast from 2.5 wt% P3HT:PCBM (Rieke Metals, Nano-C) in a 1:1 ratio in ortho-dichlorobenzene, spun at 800 rpm under nitrogen. This layer was allowed to dry overnight in a covered Petri dish and was then annealed at 110 °C for 10 min to evaporate any remaining solvent. The vacuum-deposited cathode consisted of 7 nm of Ca followed by 200 nm of Al evaporated at 10^{-6} Torr. All device areas were 7 mm^2.

Device Characterization: All photovoltaic devices were measured in the dark and under 100 mW cm^{-2} of AM 1.5G illumination, calibrated using a silicon photodiode (Newport) and corrected for the spectral mismatch of the P3HT:PCBM materials system.

Acknowledgements

The authors acknowledge H. S. Kim and Y. Cui for providing silver nanowires and Southwall Technologies for providing plastic substrates. Thanks to M. Rowell and B. Hardin for helpful discussions. This work was supported by the Center for Advanced Molecular Photovoltaics (Award No KUS-C1-015-21), made by King Abdullah University of Science and Technology (KAUST).

Received: February 11, 2011
Published online: April 29, 2011

[1] G. Haacke, *Annu. Rev. Mater. Sci.* **1977**, *7*, 73.
[2] B. G. Lewis, D. C. Paine, *MRS Bull.* **2000**, *25*, 22.
[3] B. L. Gehman, S. Jonsson, T. Rudolph, M. Scherer, M. Weigert, R. Werner, *Thin Solid Films* **1992**, *220*, 333.
[4] Z. Chen, B. Cotterell, W. Wang, E. Guenther, S.-J. Chua, *Thin Solid Films* **2001**, *394*, 201.
[5] S. K. Park, J. I. Han, D. G. Moon, W. K. Kim, *Jpn. J. Appl. Phys., Part 1* **2003**, *42*, 623.
[6] A. Kumar, C. Zhou, *ACS Nano* **2010**, *4*, 11.
[7] J. L. Blackburn, T. M. Barnes, M. C. Beard, Y. H. Kim, R. C. Tenent, T. J. McDonald, B. To, T. J. Coutts, M. J. Heben, *ACS Nano* **2008**, *2*, 1266.
[8] Z. R. Li, H. R. Kandel, E. Dervishi, V. Saini, Y. Xu, A. R. Biris, D. Lupu, G. J. Salamo, A. S. Biris, *Langmuir* **2008**, *24*, 2655.
[9] M. H. A. Ng, L. T. Hartadi, H. Tan, C. H. P. Poa, *Nanotechnolgy* **2008**, *19*, 205703.
[10] A. D. Pasquier, H. E. Unalan, A. Kanwal, S. Miller, M. Chhowalla, *Appl. Phys. Lett.* **2005**, *87*, 203511.
[11] M. W. Rowell, M. A. Topinka, M. D. McGehee, H. J. Prall, G. Dennler, N. S. Sariciftci, L. B. Hu, G. Gruner, *Appl. Phys. Lett.* **2006**, *88*, 233506.
[12] Z. C. Wu, Z. H. Chen, X. Du, J. M. Logan, J. Sippel, M. Nikolou, K. Kamaras, J. R. Reynolds, D. B. Tanner, A. F. Hebard, A. G. Rinzler, *Science* **2004**, *305*, 1273.
[13] H. c. A. Becerril, J. Mao, Z. Liu, R. M. Stoltenberg, Z. Bao, Y. Chen, *ACS Nano* **2008**, *2*, 463.
[14] J. Wu, M. Agrawal, H. A. Becerril, Z. Bao, Z. Liu, Y. Chen, P. Peumans, *ACS Nano* **2009**, *4*, 43.
[15] J. B. Wu, H. A. Becerril, Z. N. Bao, Z. F. Liu, Y. S. Chen, P. Peumans, *Appl. Phys. Lett.* **2008**, *92*, 263302.
[16] G. Eda, G. Fanchini, M. Chhowalla, *Nat. Nanotechnol.* **2008**, *3*, 270.
[17] V. C. Tung, L.-M. Chen, M. J. Allen, J. K. Wassei, K. Nelson, R. B. Kaner, Y. Yang, *Nano Lett.* **2009**, *9*, 1949.
[18] Y.-M. Chang, L. Wang, W.-F. Su, *Org. Electron.* **2008**, *9*, 968.
[19] A. Colsmann, F. Stenzel, G. Balthasar, H. Do, U. Lemmer, *Thin Solid Films* **2009**, *517*, 1750.
[20] H. Do, M. Reinhard, H. Vogeler, A. Puetz, M. F. G. Klein, W. Schabel, A. Colsmann, U. Lemmer, *Thin Solid Films* **2009**, *517*, 5900.
[21] S. K. Hau, H.-L. Yip, J. Zou, A. K. Y. Jen, *Org. Electron.* **2009**, *10*, 1401.
[22] S.-I. Na, S.-S. Kim, J. Jo, D.-Y. Kim, *Adv. Mater.* **2008**, *20*, 4061.
[23] Y. Zhou, F. Zhang, K. Tvingstedt, S. Barrau, F. Li, W. Tian, O. Inganas, *Appl. Phys. Lett.* **2008**, *92*, 233308.
[24] H. Wu, L. Hu, M. W. Rowell, D. Kong, J. J. Cha, J. R. McDonough, J. Zhu, Y. Yang, M. D. McGehee, Y. Cui, *Nano Lett.* **2010**, *10*, 4242.
[25] F. C. Krebs, *Org. Electron.* **2009**, *10*, 761.
[26] Y. Galagan, J.-E. J. M. Rubingh, R. Andriessen, C.-C. Fan, P. W. M. Blom, S. C. Veenstra, J. M. Kroon, *Sol. Energy Mater. Sol. Cells* **2011**, *95*, 1339.
[27] F. C. Krebs, *Sol. Energy Mater. Sol. Cells* **2009**, *93*, 1636.
[28] J.-Y. Lee, S. T. Connor, Y. Cui, P. Peumans, *Nano Lett.* **2008**, *8*, 689.
[29] S. De, T. M. Higgins, P. E. Lyons, E. M. Doherty, P. N. Nirmalraj, W. J. Blau, J. J. Boland, J. N. Coleman, *ACS Nano* **2009**, *3*, 1767.
[30] W. Gaynor, J. Y. Lee, P. Peumans, *ACS Nano* **2010**, *4*, 30.
[31] L. Hu, H. S. Kim, J.-Y. Lee, P. Peumans, Y. Cui, *ACS Nano* **2010**, *4*, 2955.

[32] M.-G. Kang, T. Xu, H. J. Park, X. Luo, L. J. Guo, *Adv. Mater.* **2010**, *22*, 4378.
[33] M. W. Rowell, M. D. McGehee, *Energy Environ. Sci.* **2011**, *4*, 131.
[34] Q. L. Song, F. Y. Li, H. Yang, H. R. Wu, X. Z. Wang, W. Zhou, J. M. Zhao, X. M. Ding, C. H. Huang, X. Y. Hou, *Chem. Phys. Lett.* **2005**, *416*, 42.
[35] Y. Kim, S. Cook, S. M. Tuladhar, S. A. Choulis, J. Nelson, J. R. Durrant, D. D. C. Bradley, M. Giles, I. Mcculloch, C. S. Ha, M. Ree, *Nat. Mater.* **2006**, *5*, 197.
[36] G. Li, V. Shrotriya, J. S. Huang, Y. Yao, T. Moriarty, K. Emery, Y. Yang, *Nat. Mater.* **2005**, *4*, 864.
[37] G. Li, V. Shrotriya, Y. Yao, Y. Yang, *J. Appl. Phys.* **2005**, *98*, 043704.
[38] S. H. Park, A. Roy, S. Beaupre, S. Cho, N. Coates, J. S. Moon, D. Moses, M. Leclerc, K. Lee, A. J. Heeger, *Nat. Photonics* **2009**, *3*, 297.
[39] H.-Y. Chen, J. Hou, S. Zhang, Y. Liang, G. Yang, Y. Yang, L. Yu, Y. Wu, G. Li, *Nat. Photonics* **2009**, *3*, 649.
[40] X. Yang, J. Loos, *Macromolecules* **2007**, *40*, 1353.
[41] X. Yang, J. Loos, S. C. Veenstra, W. J. H. Verhees, M. M. Wienk, J. M. Kroon, M. A. J. Michels, R. A. J. Janssen, *Nano Lett.* **2005**, *5*, 579.